T cell–derived interleukin (IL)-21 promotes brain injury following stroke in mice

Benjamin D.S. Clarkson,[1,3] Changying Ling,[1] Yejie Shi,[2] Melissa G. Harris,[1,4] Aditya Rayasam,[4] Dandan Sun,[2,5] M. Shahriar Salamat,[1] Vijay Kuchroo,[6] John D. Lambris,[7] Matyas Sandor,[1] and Zsuzsanna Fabry[1]

[1]Department of Pathology and Laboratory Medicine, [2]Department of Neurological Surgery, [3]Department of Cellular and Molecular Pathology, [4]Neuroscience Training Program, School of Medicine and Public Health, University of Wisconsin-Madison, Madison, WI 53792
[5]Veterans Affairs Pittsburgh Health Care System, Geriatric Research, Educational and Clinical Center, Pittsburgh, PA 15213
[6]Center for Neurological Diseases, Brigham and Women's Hospital Harvard Medical School, Boston, MA 02115
[7]Department of Pathology and Laboratory Medicine, University of Pennsylvania School of Medicine, Philadelphia, PA 19104

T lymphocytes are key contributors to the acute phase of cerebral ischemia reperfusion injury, but the relevant T cell–derived mediators of tissue injury remain unknown. Using a mouse model of transient focal brain ischemia, we report that IL-21 is highly up-regulated in the injured mouse brain after cerebral ischemia. IL-21–deficient mice have smaller infarcts, improved neurological function, and reduced lymphocyte accumulation in the brain within 24 h of reperfusion. Intracellular cytokine staining and adoptive transfer experiments revealed that brain-infiltrating CD4$^+$ T cells are the predominant IL-21 source. Mice treated with decoy IL-21 receptor Fc fusion protein are protected from reperfusion injury. In postmortem human brain tissue, IL-21 localized to perivascular CD4$^+$ T cells in the area surrounding acute stroke lesions, suggesting that IL-21–mediated brain injury may be relevant to human stroke.

CORRESPONDENCE
Zsuzsanna Fabry:
zfabry@facstaff.wisc.edu

Abbreviations used: BA, basilar artery; ECA, external carotid artery; ICA, internal carotid artery; I/R, ischemia/reperfusion; MCA, middle cerebral artery; PCA, posterior cerebral artery; PComA, posterior communicating artery; RAG, recombination activating gene; rCBF, regional cerebral blood flow; tMCAO, transient MCA occlusion; TTC, 2,3,5-triphenyltetrazolium chloride; VA, vertebral artery.

Stroke is one of the leading causes of death and disability worldwide. Clinical and preclinical experimental studies highlight the importance of inflammation in both acute and delayed neuronal tissue damage after ischemic stroke; however, the mechanisms and cells involved in this neuroinflammation are not fully understood. There is currently no available treatment targeting the acute immune response that develops in the brain after transient focal ischemia. Therefore, we sought to identify novel T cell–derived cytokines that contribute to acute cerebral reperfusion using the mouse model of transient middle cerebral artery occlusion (tMCAO).

During the reperfusion of infarcted brain tissue, leukocytes accumulate in the injured brain where, in addition to clearing cell debris, they promote secondary tissue injury (Yilmaz and Granger, 2010). Within the acute phase of ischemic reperfusion (I/R) injury there are multiple waves of cell infiltration of macrophages, neutrophils, and lymphocytes (Gelderblom et al., 2009). Brain-infiltrating T cells have also been widely reported in stroke and animal models of stroke and are thought to have acute detrimental and delayed protective effects (Magnus et al., 2012). Conventionally, the protective role of T cells has been attributed to the accumulation of regulatory T cells within the CNS in later stages of reperfusion injury. These T cells produce a variety of cytokines including TGFβ and IL-10, which are both antiinflammatory and neuroprotective. (Liesz et al., 2009; Stubbe et al., 2013). In addition to having an established role in delayed neuroprotection, Kleinschnitz et al. (2013) have recently shown that CD4$^+$ CD25$^+$ regulatory T cells also promote acute ischemic injury through interaction with the cerebral vasculature. The acute detrimental effects can be further divided into early (24 h) and late (72 h) phases, with IL-17 production by nonconventional γδ T cells (less common T cell subset associated with mucosal tissues) possibly accounting for the latter by promoting neutrophil accumulation (Gelderblom et al., 2012).

The mechanisms of the early detrimental effects of T cells after cerebral ischemia are least

The Rockefeller University Press $30.00
J. Exp. Med. 2014 Vol. 211 No. 4 595-604
www.jem.org/cgi/doi/10.1084/jem.20131377

understood. Several laboratories have reported reduced neurological deficit and infarct volumes at 24–48 h reperfusion in T cell–deficient mice after tMCAO (Yilmaz and Granger, 2010). After tMCAO, recombination activating gene 1–deficient (RAG1 KO) mice, which lack T and B lymphocytes, have significantly smaller brain injury compared with controls; whereas, adoptive transfer of WT $CD4^+$ helper T cells or $CD8^+$ cytotoxic T cells increases stroke infarct volumes within 24 h after ischemia in these mice (Kleinschnitz et al., 2010). Additionally, TCR-transgenic mice and mice lacking co-stimulatory TCR signaling molecules were fully susceptible to acute I/R injury, indicating that T cell involvement at early time points is antigen-independent (Kleinschnitz et al., 2010). These data demonstrate that conventional $CD4^+$ or $CD8^+$ $\alpha\beta$ T cells exacerbate acute injury after cerebral ischemia independently of TCR ligation, and this effect seems to be concomitant with an early increase in T cell infiltration into the postischemic brain, which many have reported to be between 3 and 48 h (Yilmaz et al., 2006; Gelderblom et al., 2009).

Recent findings suggest that, in the postischemic brain, within hours of reperfusion T cells accumulate in postcapillary segments of periinfarct inflamed cerebral microvasculature characterized by high endothelial expression of chemokines and adhesion molecules. These postcapillary venules have been postulated to allow accumulating immune cells to activate each other and promote platelet adhesion in a process termed thrombo-inflammation (Nieswandt et al., 2011). Much research has been devoted to identifying T cell factors that promote thrombo-inflammation (Barone et al., 1997; Hedtjärn et al., 2002; Yilmaz et al., 2006; Shichita et al., 2009; Gelderblom et al., 2012); however, to our knowledge no study has yet identified the T cell–derived factors responsible for the early increase in infarct volumes at 24 h reperfusion. Here, we present data that identify IL-21 as a key $CD4^+$ T cell–derived inflammatory factor that contributes to increased early ischemic tissue injury.

RESULTS AND DISCUSSION

Robust up-regulation of IL-21 during cerebral I/R injury

IL-21 is closely related to IL-2 and IL-15 and signals through the IL-21 receptor, which is comprised of an IL-21–specific α subunit and a common γ subunit shared with IL-2, IL-7, IL-9, and IL-15. IL-21 is known to regulate immune responses by promoting antibody production, T cell–mediated immunity, and NK cell and $CD8^+$ T cell cytotoxicity. Recently, others have shown that stress signals from necrotic tissue can induce rapid IL-21 production from naive T cells (Holm et al., 2009), and co-stimulation with TLR3 ligands during polyclonal T cell activation significantly increases IL-21 secretion that contributes to small intestine localized pediatric celiac disease (van Leeuwen et al., 2013). To test whether IL-21 is up-regulated in brain after ischemic necrosis induced by MCAO and to better understand the cytokines involved in T cell–mediated cerebral I/R injury, we measured changes in inflammatory gene expression in the brain within 24 h after tMCAO in mice using PCR-based gene array analysis. In addition to verifying the up-regulation of several previously reported inflammatory genes, we found that IL-21 was one of the most highly expressed inflammatory genes among those measured (Fig. 1 a). Gene expression levels from arrays were normalized to interquartile spot intensity. Arrays did not differ systemically in gene expression levels before or after normalization (not depicted). This increase in IL-21 gene expression was confirmed by real-time (RT) PCR analysis, which detected a >24-fold relative increase in IL-21 gene expression in the ipsilateral ischemic brain tissues compared with the contralateral hemisphere at 24 h reperfusion (Fig. 1 b). IL-21 was not detectable by this method in healthy brain tissue (Fig. 1 b).

IL-21–deficient mice are protected from acute neuronal injury after cerebral I/R injury

Whether IL-21 contributes to ischemic tissue injury had not been directly studied. However, in the last few years it has become evident that IL-21 expression is associated with acute rejection in mice after kidney, heart, or liver allograft (Baan et al., 2007; Hecker et al., 2009; Xie et al., 2010). Because these models also involve reperfusion of ischemic tissues, these findings support the potential role of IL-21 in I/R injury.

We evaluated the levels of cerebral I/R injury in IL-21–deficient (IL-21 KO) mice. Infarct volumes in IL-21 KO mice were reduced to ∼35% of the infarct volumes observed in congenic C57BL6/J WT mice as early as 24 h after tMCAO, as measured by triphenyltetrazolium chloride (TTC; Fig. 1 c). Similar effects were also seen at 4 d (not depicted) and 7 d after tMCAO (Fig. 1 d), indicating that IL-21 contributes to both immediate and delayed brain injury and suggesting that in the absence of IL-21 tissue repair can occur. Analysis of intracranial vascular anatomy revealed no differences between WT and IL-21 KO mice in the patency of the posterior communicating artery that would account for the observed differences in tissue injury (Fig. 1 g). Nor did we observe differences between WT and IL-21 KO mice in heart rate, or blood pressure before or after tMCAO (Fig. 1 h). WT and IL-21 KO $CD4^+$ T cells, $CD8^+$ T cells, and $CD11b^+$ myeloid cells showed no difference in IL-2, IL-17A, IFN-γ, or TNF production when stimulated in vitro (Fig. 2, g–l). The reduction in infarct volumes corresponded with less weight loss (unpublished data), less spleen atrophy (Fig. 2 c), and improved neurological functioning in IL-21 KO mice compared with WT mice as assessed by both grip strength (Fig. 1 e) and Bederson (Fig. 1 f) scoring 1, 4, and 7 d after tMCAO.

We measured accumulation of monocytes and lymphocytes in the brain after tMCAO in IL-21 KO and WT animals (gating strategy in Fig. 2 a). We did not observe significant differences in the rate of accumulation of monocytes ($CD45^{high}$ $CD11b^+Ly6c^{high}$), microglia ($CD45^{int}CD11b^+$), B cells ($B220^+$), $\gamma\delta$ T cells ($\gamma\delta TCR^+$), NK, or NKT cells ($NK1.1^+$) in the ischemic brain of WT and IL-21 KO mice after 1, 4, and 7 d of reperfusion (unpublished data). In contrast, as early as 1 d after tMCAO, IL-21 KO mice showed significantly diminished cerebral accumulation of $CD4^+$ T cells and $CD8^+$ T cells

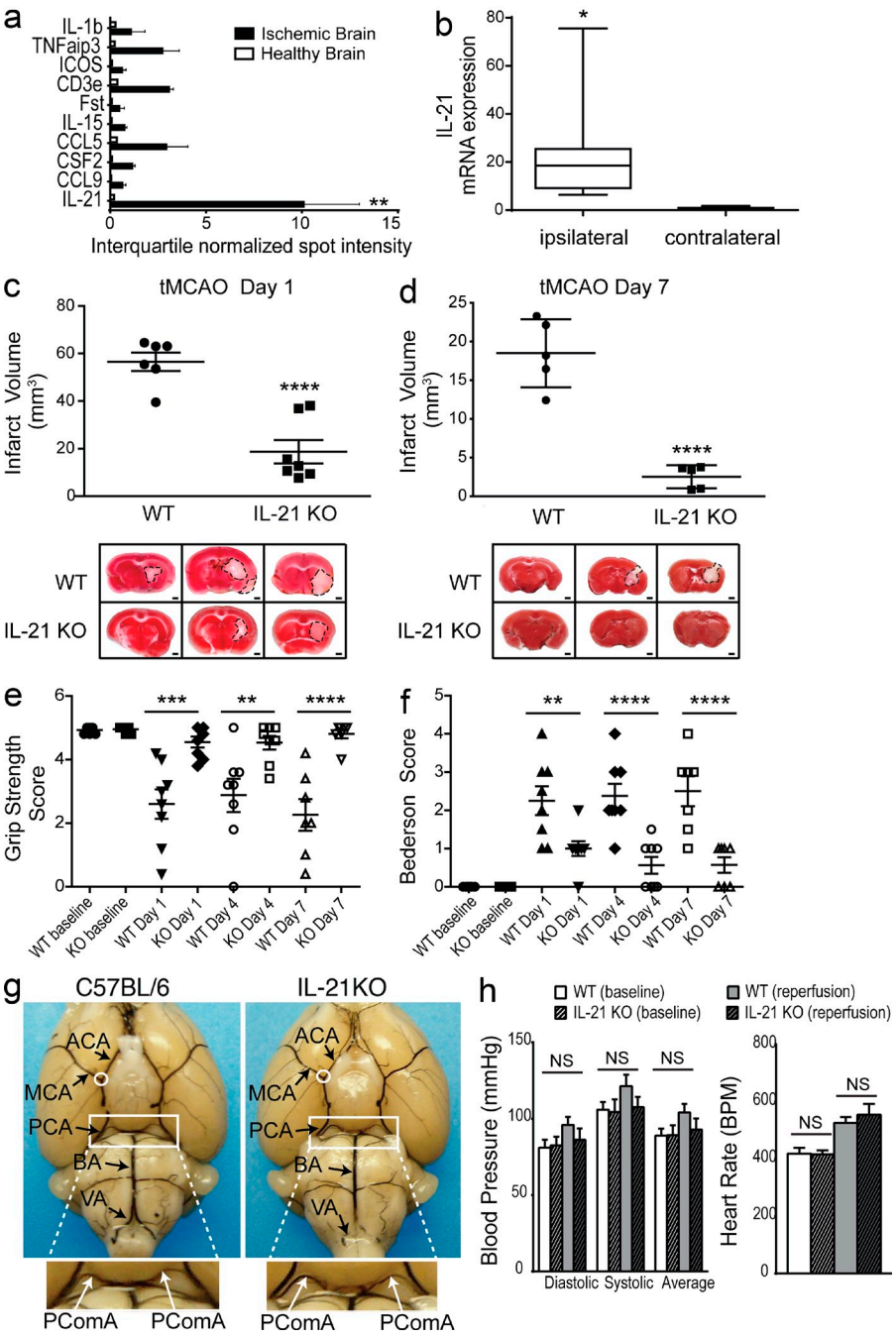

Figure 1. IL-21 is up-regulated early in mouse brain, and IL-21–deficient mice are protected after tMCAO. GeArray S Series Mouse Autoimmune and Inflammatory Response gene array of transcripts expressed in pooled brain tissues 24 h after tMCAO or sham procedure (n = 3–6 mice per group). (a) Bar graphs show PCR array spot intensity of genes with a greater than sixfold difference in gene expression in tMCAO compared with sham, normalized to the interquartile mean spot intensity. (b) IL-21 mRNA expression level in ipsilateral hemisphere relative to contralateral hemisphere 24 h after tMCAO (n = 3 per group). Mann-Whitney rank sum test *, $P < 0.05$. Plots show median, lower, and upper quartile (box) and range (error bars). Infarct volumes of WT and IL-21 KO mice 24 h after tMCAO (c) and 7 d after tMCAO (d). Representative images of TTC-stained 2-mm brain slices shown below (n = 5–7 mice per group). WT and IL-21 KO mice grip strength (e) and Bederson score (f) at 1, 4, and 7 d after 1 h tMCAO (n = 7–8 for each group). (g) Brain vasculature of C57BL/6 and IL-21KO mice perfused transcardially with carbon lampblack (C198-500; Thermo Fisher Scientific) in 20% gelatin dd$H_2$0. Arrows indicate anterior cerebral (ACA), MCA, posterior cerebral (PCA), basilar (BA), and vertebral arteries (VA), showing point of occlusion (white circle). High magnification images demonstrate no difference in patency of the posterior communicating artery (PComA, arrows). (h) Heart rate and blood pressure of WT and IL-21 KO mice before and after tMCAO (n = 3–4 mice per group). Data are representative of 2–3 independent experiments. **, $P < 0.01$; ***, $P < 0.001$; ****, $P < 0.0001$ by Student's t test (single comparison) or one-way ANOVA (multiple comparisons). Error bars indicate SD.

after tMCAO compared with WT mice (Fig. 2 e) and these differences persisted at day 7 (Fig. 2 f). These differences were not reflected in the spleen before or after tMCAO (Fig. 2 b). IL-21 has also been shown to be produced by and modulate the function of regulatory T cells (Peluso et al., 2007; Battaglia et al., 2013), which begin to accumulate in the brain after tMCAO. Thus, we compared the frequency of regulatory CD4 T cells expressing the marker Foxp3 in the brain and spleen 24 h after tMCAO in WT and IL-21 KO mice. IL-21 KO mice exhibited no difference in regulatory T cell abundance in either tissue compared with WT experimental animals. Nor did we observe a difference between WT and IL-21 KO mice in the frequency of lymphocytes producing the antiinflammatory cytokine IL-10 among B cells ($B220^+$), $CD8^+$ T cells, or $CD4^+$ T cells (unpublished data). These data demonstrate that IL-21 deficiency is protective at acute time points after tMCAO and IL-21 levels in the CNS correlate with early infiltration of T cells without affecting regulatory T or B cell accumulation or IL-10 cytokine production during the acute period (day 1–4).

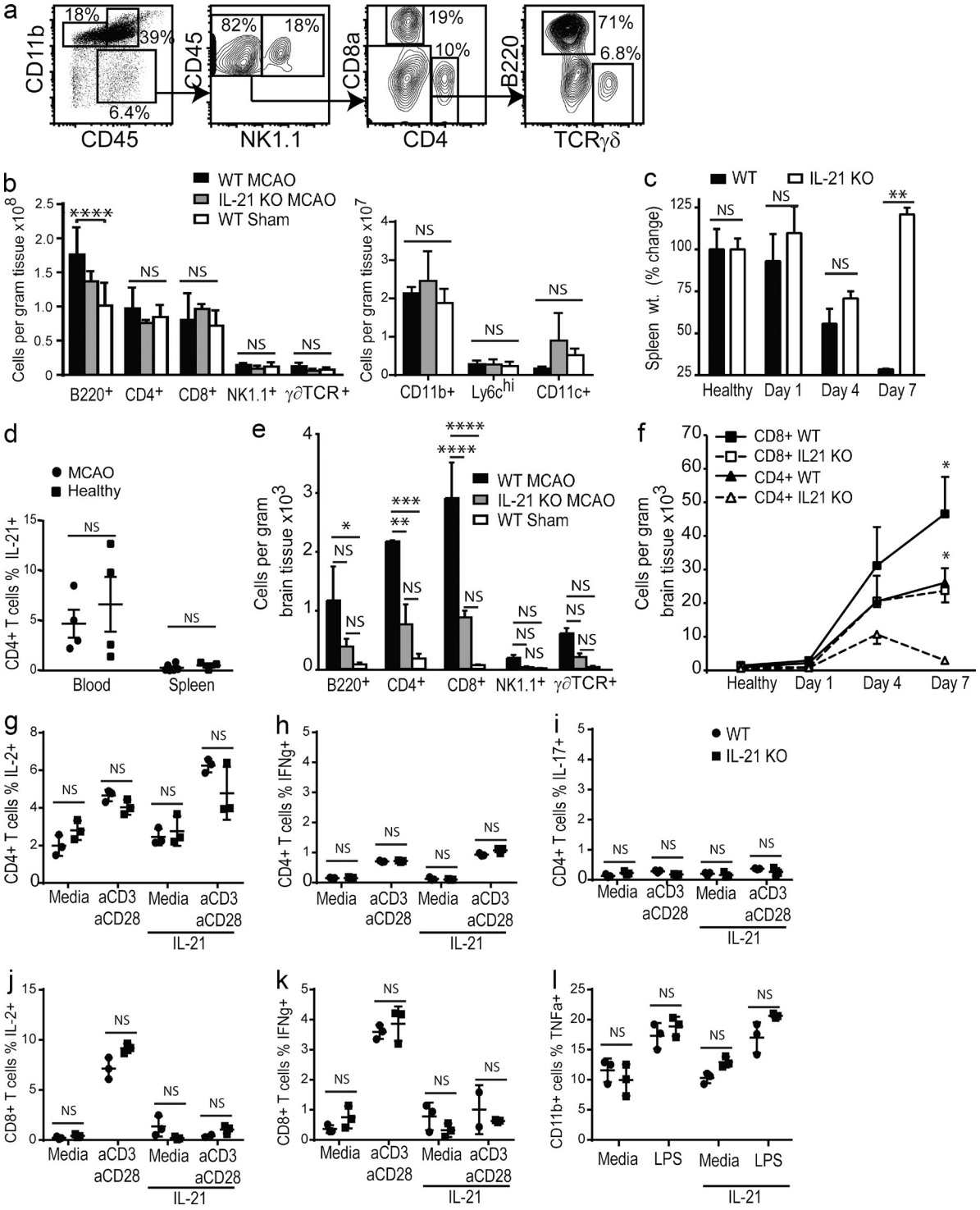

Figure 2. Lymphocyte recruitment to brain is diminished in IL-21 deficient mice. (a) Gating strategy for leukocytes isolated from brain after MCAO. (b) WT and IL-21 KO spleen cells 24 h after tMCAO or sham procedure ($n = 3$ mice per group). (c) Relative change in spleen weight of WT and IL-21 KO mice after tMCAO ($n = 3$–7 mice per group). (d) Percentage of blood and spleen CD4$^+$ T cells expressing IL-21 after 5-h ex vivo stimulation with PMA (10 ng/ml) and Ionomycin (1 µg/ml) 4 d after MCAO or control treatment. (e and f) Leukocyte accumulation in the brain of WT mice compared with IL-21 KO mice 1, 4, and 7 d after tMCAO ($n = 3$–6 mice per group). (g–k) In vitro cytokine expression by WT and IL-21 KO CD4$^+$ and CD8α^+ T cells after 5-h stimulation under indicated conditions with or without recombinant mouse IL-21 (100 ng/ml). (l) TNF production by CD11b$^+$ myeloid cells stimulated with LPS (500 ng/ml) for 5 h with or without recombinant mouse IL-21 (100 ng/ml). Cells isolated from $n = 3$ mice per group. Data are representative of two to four independent experiments. *, $P < 0.05$; **, $P < 0.01$; ***, $P < 0.001$; ****, $P < 0.0001$ by Student's t test (single comparison) or one-way ANOVA (multiple comparisons). Error bars indicate SD (b–d and g–l) and SEM (e, f).

IL-21 is primarily produced by brain-infiltrating CD4+ T cells

We measured intracellular IL-21 production by various cell populations. IL-21–producing cells were not detected by flow cytometry among cells isolated from healthy brain, but could be detected among mononuclear cells isolated from ischemic brain 24 h after tMCAO. Gating on IL-21+ cells revealed that the majority of these cells were CD4+ T cells (Fig. 3 a). IL-21–producing CD4+ T cells were also detected at low levels among cells isolated from blood, but not spleen, of healthy WT mice, and these levels were unaffected after transient cerebral ischemia (Fig. 2 d), indicating that the increase in IL-21 production was limited to CD4+ T cells recovered from the postischemic brain. Next, we adoptively transferred WT or IL-21 KO CD4+ T cells into lymphocyte-deficient RAG2 KO mice. Purity of transferred CD4+ T cells was confirmed by flow cytometry to be ∼95% (Fig. 3 b). As shown previously (Kleinschnitz et al., 2010), we observed markedly reduced infarcts in RAG KO mice compared with WT mice, and infarct volumes could be restored to WT levels in RAG2 KO by adoptively transferring WT CD4+ T cells. Most importantly, RAG2 KO mice that received WT CD4+ T cells had significantly larger infarcts than those receiving IL-21 KO CD4+ T cells (Fig. 3 c).

IL-21 blockade is protective in tMCAO

We treated WT mice with IL-21 receptor Fc protein (IL-21R.Fc) using a previously described protocol (Jang et al., 2009; McGuire et al., 2011; Spolski et al., 2012). We administered 500 µg of IL-21R.Fc i.p. 1 h before tMCAO. As measured by TTC staining, treated mice showed significantly reduced infarct volumes compared with control-treated mice 24 h after tMCAO (Fig. 4 a). We found a similarly protective effect in mice treated with IL-21R.Fc protein (500 µg i.p.) 2 h after initiation of reperfusion (Fig. 4 a). These differences were associated with decreased locomotor function (decreased resistance to lateral push and increased circling behavior) in control-treated mice compared with those treated with IL-21R.Fc (Fig. 4 b and Video 1). Although we cannot exclude the possibility that IL-21R.Fc exhibits its blocking effect in peripheral immune compartments, using ELISA for human IgG4 we were able to observe that—upon i.p. injection—soluble IL-21R.Fc accumulates in the CNS of mice after tMCAO (Fig. 4 c).

IL-21 presence localizes with CD4 staining in human stroke tissue

IL-21+ cells were recently detected in human brain tissue during different neuroinflammatory conditions (Tzartos et al., 2011). Thus, we stained groups of postmortem brain tissue from

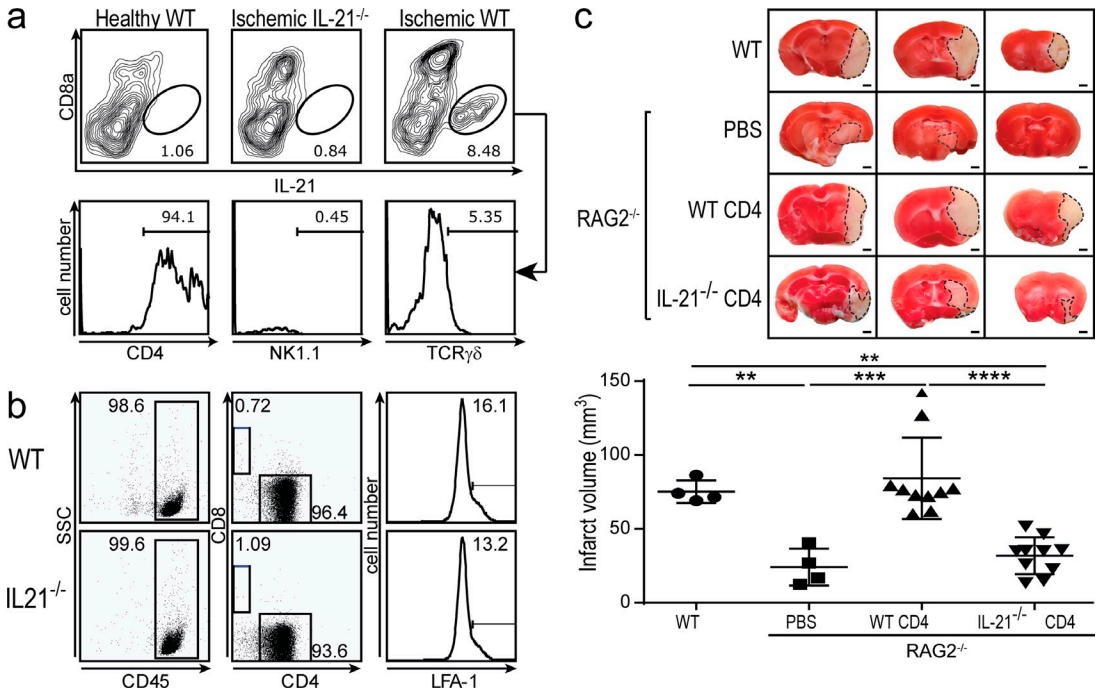

Figure 3. IL-21 is primarily produced by brain-infiltrating CD4+ T cells. (a) Intracellular cytokine staining of lymphocytes isolated from $n = 5$ pooled healthy WT, ischemic IL-21$^{-/-}$, or ischemic WT mouse brains 24 h after tMCAO or sham procedure showing IL-21 versus CD8α expression. Histograms show CD4, NK1.1, and TCRγδ expression on IL-21+ cells from ischemic WT brain. (b) CD45, CD4, and LFA-1 expression by negative fractions purified from WT and IL-21$^{-/-}$ lymph node cells by CD4+ negative selection using magnetic cell separation before transfer into RAG2$^{-/-}$ recipients. (c) Infarct volume in WT mice ($n = 4$), RAG2$^{-/-}$ mice ($n = 4$), RAG2$^{-/-}$ mice + WT CD4 T cells ($n = 10$), and RAG2$^{-/-}$ mice + IL-21$^{-/-}$ CD4 T cells ($n = 10$) 24 h after tMCAO. Representative TTC-stained 2-mm mouse brain slices shown on top. Data are representative of two independent experiments. **, $P < 0.01$; ***, $P < 0.001$; ****, $P < 0.0001$ one-way ANOVA. Error bars indicate SD.

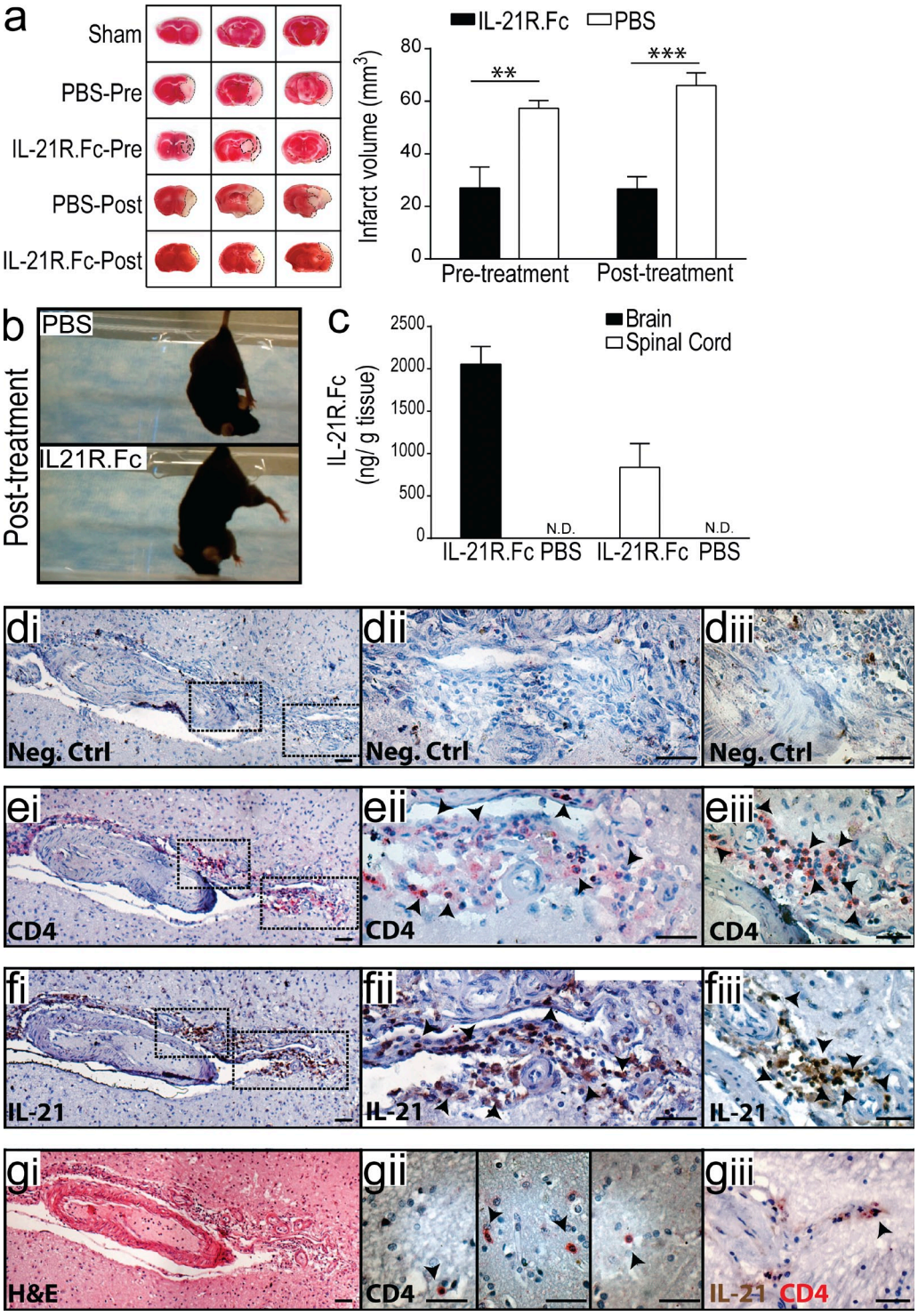

Figure 4. Blockade of IL-21 signaling before or after tMCAO reduces infarct size in WT mice. (a) Infarct volumes 24 h after tMCAO in WT mice treated with 500 µg recombinant mIL-21R.Fc or PBS 1 h before (pretreatment) or 2 h after (posttreatment) surgery. Representative TTC-stained brain slices shown on left (n = 3–4 mice per group). (b) Still image from Video 1 depicting behavioral differences between WT mice posttreated with IL-21R.Fc or PBS. (c) IL-21R.Fc protein levels in the indicated organs 20–24 h after tMCAO in WT mice injected with 500 µg IL-21R.Fc 2 h after start of reperfusion (n = 2–4 mice per group). N.D., not detected. Data are representative of two independent experiments. **, $P < 0.01$; ***, $P < 0.001$, by Student's t test. Error bars indicate SEM. Representative images of postmortem paraffin-embedded human acute stroke lesions stained with control sera (d), or primary antibodies against CD4 (e and g [ii-iii]), IL-21 (f and g [iii]), or eosin (g [i]) visualized with Fast Red (d, e, and g) and/or DAB (d, f, and g [iii]) and counterstained with hematoxylin. High magnification images are shown on right. Arrows indicate positive staining. Bars, 50 µm.

patients with acute and chronic stroke lesions. In acute infarcts, rare CD4+ T cells were found in the necrotic brain parenchyma (Fig. 4 g, ii, arrows), which was predominantly infiltrated by foamy macrophages (Fig. 4 g, i). In contrast, CD4+ T cells were consistently found within the Virchow Robins space of vessels bordering acute infarcts (not depicted) and in the subarachnoid space adjacent to meningeal vessels (arrows, Fig. 4 e, i). IL-21 staining was limited almost exclusively to these perivascular spaces. Compared with control stained tissue (Fig. 4 d, i), anti–IL-21 staining labeled cells extensively in the subarachnoid space of deep sulci penetrating the infarcted tissue—showing a similar distribution to CD4+ cells in serial sections (arrows, Fig. 4 f). Additionally, double staining with antibodies for CD4 and IL-21 revealed the presence of CD4+ IL-21+ cells in this perivascular niche (arrow, Fig. 4 g, iii). In summary, CD4+ T cells that can secrete IL-21 were detected within the CSF-filled subarachnoid and perivascular spaces during cerebral infarction in humans.

Neuronal cells express IL-21 receptor and up-regulate autophagy genes in response to IL-21

RT-PCR analysis of primary mouse neurons and murine neuronal cell lines (Neuro2A) indicated that IL-21R expression was higher on neuronal cells than on other brain cells, including astrocytes and endothelial cells (Fig. 5, a and c). This is consistent with another report where in situ hybridization detected neuron-restricted IL-21R expression in inflamed human brain tissue (Tzartos et al., 2011). Moreover, treating Neuro2a cells with IL-21 after in vitro oxygen glucose deprivation (OGD) significantly increased cell death as measured by XTT cell

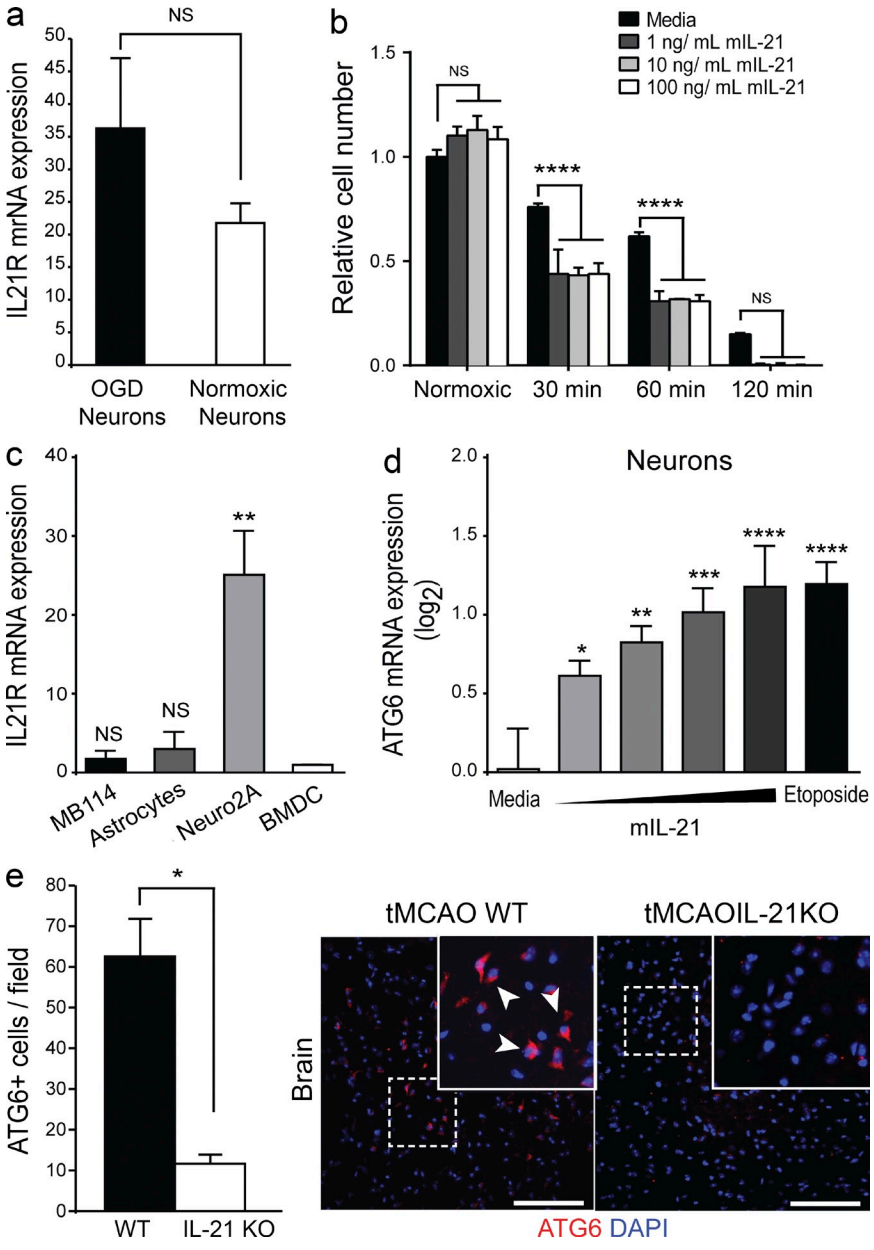

Figure 5. IL-21 promotes autophagy expression in neuronal cells after hypoxia/ischemia. (a) Il21r mRNA expression relative to GAPDH expression levels is shown in normoxic and hypoxic primary mouse neurons after OGD or control treatment. (b) Viability of Neuro2A cells treated with the indicated doses of IL-21 after OGD. (c) Il21r mRNA expression relative to GAPDH in neuronal (Neura2A), astrocytic, and endothelial cell lines (MB114) expressed relative to BMDC expression. (d) ATG6 expression in primary neurons treated with PBS, etoposide, or 32–256 ng/ml rIL-21 for 4 h after 1–2 h oxygen glucose deprivation as measured by RT-PCR. Cells treated in triplicate. (e) Number of ATG6+ cells per field in the same regions of WT and IL-21 KO mouse brains after tMCAO as assessed by immune staining (n = 3 mice per group). Arrows indicate ATG-6+ cells in periinfarcted brain tissue of WT and IL-21 KO mice. Bars, 100 µm. Data are representative of two independent experiments. *, $P < 0.05$; **, $P < 0.01$; ***, $P < 0.001$; ****, $P < 0.0001$ by Student's t test (single comparison) or one-way ANOVA (multiple comparisons). Error bars indicate SEM.

viability assay (Fig. 5 b). In subsequent studies we found that treatment of primary neurons with IL-21 up-regulated mRNA levels of the autophagy associated gene ATG6 (Fig. 5 d). These data suggest that IL-21 could directly affect neuronal autophagy during ischemic injury, which has been implicated in neuronal death in infarcted and periinfarcted brain tissue. Thus, we stained WT and IL-21 KO postischemic brain tissues for ATG6. We observed significantly fewer $ATG6^+$ cells in infarcted brain tissue of IL-21 KO mice compared with WT, suggesting that IL-21 may contribute to increased cerebral autophagy after stroke (Fig. 5 e).

In conclusion, we implicate IL-21 as a lymphocyte-derived factor with a pronounced effect on brain injury after focal ischemia in mice. We also present data demonstrating that IL-21–producing $CD4^+$ T cells are present in the brain of patients with acute stroke. These data warrant investigation of the therapeutic potential of IL-21–modifying treatments in isolation and combination with current anti-thrombotic treatments for ischemic stroke.

MATERIALS AND METHODS

Ethics statement. C57BL/6 WT mice were obtained from The Jackson Laboratory. IL-21–deficient mice ($IL\text{-}21^{tm1Lex}$) were purchased from the Mutant Mouse Regional Resources Center. All mice underwent 1 h tMCAO and 24 h reperfusion. All animal procedures used in this study were conducted in strict compliance with the National Institutes of Health Guide for the Care and Use of Laboratory Animals and approved by the University of Wisconsin Center for Health Sciences Research Animal Care Committee. All mice (~25 g) were anesthetized with 5% halothane for induction and 1.0% halothane for maintenance vaporized in N_2O and O_2 (3:2), and all efforts were made to minimize suffering.

Regional cerebral blood flow (rCBF) measurement. Changes in rCBF at the surface of the left cortex were recorded using a blood perfusion monitor (Laserflo BPM2; Vasamedics) with a fiber optic probe (0.7 mm diam). The tip of the probe was fixed with glue on the skull over the core area supplied by the MCA (2 mm posterior and 6 mm lateral from bregma). Changes in rCBF after MCAO were recorded as a percentage of the baseline value. Mice included in these investigations had >80% relative decrease in rCBF during MCAO.

Investigation of intracranial vasculature. WT and IL-21 KO mice were anesthetized with ketamine (100 mg/kg, i.p.) and xylazine (10 mg/kg, i.p.). After thoracotomy was performed, a cannula was introduced into the ascending aorta through the left ventricle. Transcardial perfusion fixation was performed with 2 ml saline and 2 ml of 3.7% formaldehyde. Carbon lampblack (C198-500; Thermo Fisher Scientific) in an equal volume of 20% gelatin in ddH_2O (1 ml) was injected through the cannula. The brains were removed and fixed in 4% PFA overnight at 4°C. Posterior communicating arteries (PComA) connect vertebrobasilar arterial system to the Circle of Willis and internal carotid arteries, and its development affects brain sensitivity to ischemia among different mouse strains (Barone et al., 1993). Development of PComA in both hemispheres was examined and graded on a scale of 0–3, as reported previously (Majid et al., 2000). 0, no connection between anterior and posterior circulation; 1, anastomosis in capillary phase (present but poorly developed); 2, small truncal PComA; 3, truncal PComA.

Focal ischemia model. Focal cerebral ischemia in mice was induced by occlusion of the left MCA, as described previously (Longa et al., 1989). Operators performing surgeries were masked to experimental groups. In brief, the left common carotid artery was exposed, and the occipital artery branches of the external carotid artery (ECA) were isolated and coagulated. After coagulation of the superior thyroid artery, the ECA was dissected distally and coagulated along with the terminal lingual and maxillary artery branches. The internal carotid artery (ICA) was isolated, and the extracranial branch of the ICA was then dissected and ligated. A standardized polyamide resin glue-coated 6.0 nylon monofilament (3021910; Doccol Corp) was introduced into the ECA lumen, and then advanced ~9–9.5 mm in the ICA lumen to block MCA blood flow. During the entire procedure, mouse body temperature was kept between 37 and 38°C with a heating pad. The suture was withdrawn 60 min after occlusion. The incision was closed, and the mice underwent recovery.

Infarction size measurement. After 24 h reperfusion, mice were sacrificed and brains were removed and frozen at −80°C for 5 min. 2-mm coronal slices were made with a rodent brain matrix (Ted Pella, Inc.). The sections were stained for 20 min at 37°C with 2% TTC (Sigma-Aldrich). Infarction volume was calculated with the method reported by Swanson et al. (1990) to compensate for brain swelling in the ischemic hemisphere. In brief, the sections were scanned, and the infarction area in each section was calculated by subtracting the noninfarct area of the ipsilateral side from the area of the contralateral side with National Institutes of Health image analysis software, ImageJ. Infarction areas on each section were summed and multiplied by section thickness to give the total infarction volume.

Gene array and RT-PCR. Ipsilateral brain hemispheres were dissected and stored in RNAlater (QIAGEN) at 4°C until further use. Total RNA was extracted and purified with RNeasy Protect Mini kit (QIAGEN) according to the manufacturer's instructions. Purified RNA samples were analyzed by GeArray S Serious Mouse Autoimmune and Inflammatory Gene array (SuperArray; Bioscience Corporation). Results from GeArray were filtered for genes with spot intensities higher than the mean local background of the bottom 75% of nonbleeding spots. For RT-PCR, 1 μg total RNA from each sample was reverse transcribed using SuperScript II first strand cDNA synthesis kit (Invitrogen). RT-PCR was performed on a Smart Cycler (Model SC 100–1; Cepheid) using IL-21 TaqMan gene expression assay (Mm00517640_m1; Applied Biosystems), RT^2 qPCR Primer assay for mouse Becn1 (PPM32434A; SABiosciences), or RT^2 qPCR Primer Assay for Mouse IL21r (PPM03762A; SABiosciences). The data were normalized to an internal reference gene, GAPDH.

Mononuclear cell isolation and flow cytometry. Brains were removed from perfused animals, weighed, minced, transferred to Medicon inserts, and ground in a MediMachine (BD) for 20–30 s. The cell suspension was washed with HBSS, and cells were resuspended in 70% Percoll (Pharmacia) and overlaid with 30% Percoll. The gradient was centrifuged at 2,250 *g* for 30 min at 4°C without brake. The interface was removed and washed once for further analysis. CD11b-positive and -negative fractions were isolated using Imag anti-CD11b magnetic particles (BD), following the manufacturer's protocol. A total of 10^6 cells were incubated for 30 min on ice with saturating concentrations of labeled antibodies with 40 μg/ml unlabeled 2.4G2 mAb to block binding to Fc receptors, and then washed 3 times with 1% BSA in PBS.

Single-cell suspensions from various tissues were cultured at 37°C in 10% FBS in RPMI 1640 media supplemented with GolgiStop (BD) in the presence of either phorbol myristate acetate (50 ng/ml) and ionomycin (1 μg/ml) for 5 h. After surface staining with antibodies against CD4, NK1.1, and γδTCR, cell suspensions were fixed and permeabilized by Cytofix/Cytoperm solution (BD), followed by staining with anti–IL-21 antibodies. Fluorochrome-labeled antibodies against CD45, CD11b, Ly6c, B220, CD4, CD8a, NK1.1, IFN-γ, and appropriate isotype controls were purchased from BD. Fluorochrome-labeled antibody against IL-21 and γδTCR was purchased from eBioscience. Cell staining was acquired on a FACSCalibur or LSRII (BD) and analyzed with FlowJo (Tree Star) software version 5.4.5.

Neurofunctional assessment. Neuromuscular coordination was assessed by grip strength test, as previously described (Kleinschnitz et al., 2010). For this test, mice were placed on a horizontal string midway between two supports. Mice were scored from 0 to 5 as follows: 0, falls off within 2 s; 1, hangs on with

forepaw(s); 2, hangs on with forepaws and moves laterally on string; 3, hangs onto string with forepaws and hindpaw(s); 4, hangs onto string with forepaws, hindpaw(s) and tail; 5, escape to supports. Mice were allowed to rest between trials. Scores for each mouse were determined by averaging 5–10 trials (each lasting ~15 s). Global neurological deficit was determined by a modified Bederson scoring system: 0, no deficit; 1, forelimb flexion; 2, unidirectional circling after being lifted by tail; 3, spontaneous unidirectional circling; 4, longitudinal rolling upon being lifted by tail; 5, spontaneous longitudinal rolling.

Generation of IL-21 receptor Fc fusion protein. Chinese hamster ovary cell line (Korn et al., 2007) expressing the extracellular domain (aa 20–236) of mouse IL-21R fused to the fragment crystallizable (Fc) portion of human IgG4 (IL-21R.Fc) were maintained in UltraCHO (BioWhittaker). IL-21R.Ig was purified from the culture supernatant by passage through a protein G–Sepharose column and concentrated by ultrafiltration. Concentration was determined spectrophotometrically. Purity and molecular weight were confirmed by sodium dodecyl-sulfate PAGE and human-IgG4 ELISA (eBioscience) following the manufacturer's instructions. The IL-21R.Fc reagent was tested in vitro for its ability to suppress IL-21–induced T cell proliferation.

Immunohistochemistry. Paraffin-embedded postmortem brain tissue sections from individuals with acute and chronic stroke lesions were obtained from the Neuropathology Laboratory of the University of Wisconsin Department of Pathology. After rehydration and deparaffinization, sections underwent heat-induced antigen retrieval in 10 mM sodium citrate, pH 6.0, for surface antigens or Tris-EDTA (10 mM/1 mM) with 0.05% Tween-20 for intracellular antigens. Sections were blocked for 30 min with secondary serum (10% in Tris-buffered saline) and then stained with primary antibodies, 0.5% chicken anti–IL-21 (Lifespan Biosciences) or prediluted mouse anti-CD4 ([1F6]; ab17131; Abcam) for 1–2 h at 37°C or overnight at 4°C. Normal primary sera (5–10%) were used for negative control. After several washes, secondary antibodies (biotin-labeled goat anti–chicken or biotin-labeled goat anti–mouse;Vector Laboratories) were applied to sections and incubated for 2 h at room temperature. Staining was developed using the VECTASTAIN ABC-HRP kit (Vector Laboratories) with diaminobenzidine substrate (BD) or streptavidin-alkaline phosphatase with Fast Red substrate (Laboratory Vision), following the manufacturer's instructions. Slides were lightly counterstained with hematoxylin, rinsed with running tap water, and mounted. For frozen mouse sections WT and IL-21 KO mice underwent 1-h tMCAO and 1–7-d reperfusion. Brains were perfused with PBS and 3% formalin, embedded in OCT, and cut into 8-µm frozen sections for immunohistochemistry. Frozen sections were thawed for 10 min at room temperature and blocked with 5% goat serum solution in PBS for 15 min. Sections were stained with rabbit polyclonal antibodies for ATG6 for 1 h at room temperature, followed by phycoerythrin-labeled goat anti–rabbit IgG (Santa Cruz Biotechnology, Inc.). Images were acquired on a BX40 microscope equipped with a Q-Color 3 camera using Q-Capture software (Olympus). Digital images were processed and analyzed using Photoshop CS4 software (Adobe). Color balance, brightness, and contrast settings were manipulated to generate final images. All changes were applied equally to entire image.

Neuronal cell oxygen glucose deprivation. Primary neuronal cultures derived from embryonic day 14–18 mouse cortices were grown to 80% confluency in neural basal media supplemented with B27 (2%) and penicillin/streptomycin (1%), as previously described (Kintner et al., 2010). Astrocytic and microglial contamination was excluded based on the absence of $GFAP^+$ and $CD11b^+$ cells when stained by immunocytochemistry. For OGD, media was replaced with neural basal media with or without glucose and placed in a hypoxic chamber or under normoxic conditions for 2 h at 37°C. Afterward, cells were lysed and mRNA isolated using RNeasy mini kit (QIAGEN). For XTT viability assay, Neuro2A underwent OGD and were treated with dose curve of IL-21 immediately after return to normoxic media and incubated for 4 h at 37°C. XTT labeling mixture (50 µl per well; Roche) was added according to manufacturer's instructions, and at18 h fluorescence was read on a GENious Microplate reader (Tecan). Cell number was calculated using a standard curve of known untreated cells kept under normoxic conditions.

Statistical analyses and quality standards. All surgeries were performed in a blinded manner by a third party and measurements masked where possible. Infarct volume measurements from TTC stained sections were averaged from two to three independent blinded observers. Based on power calculations, $n = 3$–10 sex- and age-matched mice were used for each experiment and group assignment was randomized. Among animals receiving MCAO procedure, 86.5% of WT mice, 93.5% of IL-21KO mice, and 100% of RAG2KO mice were included in analysis. Mice were excluded due to premature death (13.5% of WT mice, 3.2% of IL-21 KO mice) or vessel variation (3.2% of IL-21KO mice). Results are given as means ±1 SD. Multiple comparisons were made using one-way ANOVA. Where appropriate, two-tailed Student's *t* test analysis was used for comparing measures made between two groups. For comparison of RT-PCR data, nonparametric Mann-Whitney rank sum analysis was used. P-values <0.05 were considered significant.

Online supplemental material. Video 1 shows groups of WT C57BL6 mice treated with 500 µg IL-21R.Fc or PBS control via i.p. injection. Online supplemental material is available at http://www.jem.org/cgi/content/full/jem.20131377/DC1.

We thank Satoshi Kinoshita for expert histopathology services, Guoqing Song for assisting in the surgical procedures, Dr. Wenda Gao for providing reagents and protocols for the purification of IL-21R.Fc protein, and members of our laboratory for helpful discussions and constructive criticisms of this work. We also thank Khen Macvilay and Sinarack Macvilay for their expertise provided for cytofluorimetry and immunohistochemistry studies and Samuel (Joe) Ollar for assisting in the OGD procedure.

This work was supported by awards from the American Heart Association (predoctoral fellowship #12PRE12060020 to B.D.S. Clarkson) and the National Institutes of Health (NS037570 and NS076946 to ZF, AI048087 to M.S. Salamat, and AI068730 to J.D. Lambris).

The authors have no competing financial interests.

Submitted: 1 July 2013
Accepted: 24 February 2014

REFERENCES

Baan, C.C., A.H. Balk, I.E. Dijke, S.S. Korevaar, A.M. Peeters, R.P. de Kuiper, M. Klepper, P.E. Zondervan, L.A. Maat, and W. Weimar. 2007. Interleukin-21: an interleukin-2 dependent player in rejection processes. *Transplantation*. 83:1485–1492. http://dx.doi.org/10.1097/01.tp.0000264998.23349.54

Barone, F.C., D.J. Knudsen, A.H. Nelson, G.Z. Feuerstein, and R.N. Willette. 1993. Mouse strain differences in susceptibility to cerebral ischemia are related to cerebral vascular anatomy. *J. Cereb. Blood Flow Metab.* 13:683–692. http://dx.doi.org/10.1038/jcbfm.1993.87

Barone, F.C., B. Arvin, R.F. White, A. Miller, C.L. Webb, R.N. Willette, P.G. Lysko, and G.Z. Feuerstein. 1997. Tumor necrosis factor-alpha. A mediator of focal ischemic brain injury. *Stroke*. 28:1233–1244. http://dx.doi.org/10.1161/01.STR.28.6.1233

Battaglia, A., A. Buzzonetti, C. Baranello, M. Fanelli, M. Fossati, V. Catzola, G. Scambia, and A. Fattorossi. 2013. Interleukin-21 (IL-21) synergizes with IL-2 to enhance T-cell receptor-induced human T-cell proliferation and counteracts IL-2/transforming growth factor-β-induced regulatory T-cell development. *Immunology*. 139:109–120. http://dx.doi.org/10.1111/imm.12061

Gelderblom, M., F. Leypoldt, K. Steinbach, D. Behrens, C.U. Choe, D.A. Siler, T.V. Arumugam, E. Orthey, C. Gerloff, E. Tolosa, and T. Magnus. 2009. Temporal and spatial dynamics of cerebral immune cell accumulation in stroke. *Stroke*. 40:1849–1857. http://dx.doi.org/10.1161/STROKEAHA.108.534503

Gelderblom, M., A. Weymar, C. Bernreuther, J. Velden, P. Arunachalam, K. Steinbach, E. Orthey, T.V. Arumugam, F. Leypoldt, O. Simova, et al. 2012. Neutralization of the IL-17 axis diminishes neutrophil invasion and protects from ischemic stroke. *Blood*. 120:3793–3802. http://dx.doi.org/10.1182/blood-2012-02-412726

Hecker, A., A. Kaufmann, M. Hecker, W. Padberg, and V. Grau. 2009. Expression of interleukin-21, interleukin-21 receptor alpha and related type I cytokines by intravascular graft leukocytes during acute renal allograft

rejection. *Immunobiology*. 214:41–49. http://dx.doi.org/10.1016/j.imbio.2008.04.004

Hedtjärn, M., A.L. Leverin, K. Eriksson, K. Blomgren, C. Mallard, and H. Hagberg. 2002. Interleukin-18 involvement in hypoxic-ischemic brain injury. *J. Neurosci*. 22:5910–5919.

Holm, C.K., C.C. Petersen, M. Hvid, L. Petersen, S.R. Paludan, B. Deleuran, and M. Hokland. 2009. TLR3 ligand polyinosinic:polycytidylic acid induces IL-17A and IL-21 synthesis in human Th cells. *J. Immunol*. 183:4422–4431. http://dx.doi.org/10.4049/jimmunol.0804318

Jang, E., S.H. Cho, H. Park, D.J. Paik, J.M. Kim, and J. Youn. 2009. A positive feedback loop of IL-21 signaling provoked by homeostatic CD4+CD25- T cell expansion is essential for the development of arthritis in autoimmune K/BxN mice. *J. Immunol*. 182:4649–4656. http://dx.doi.org/10.4049/jimmunol.0804350

Kintner, D.B., X. Chen, J. Currie, V. Chanana, P. Ferrazzano, A. Baba, T. Matsuda, M. Cohen, J. Orlowski, S.Y. Chiu, et al. 2010. Excessive Na+/H+ exchange in disruption of dendritic Na+ and Ca2+ homeostasis and mitochondrial dysfunction following in vitro ischemia. *J. Biol. Chem*. 285:35155–35168. http://dx.doi.org/10.1074/jbc.M110.101212

Kleinschnitz, C., N. Schwab, P. Kraft, I. Hagedorn, A. Dreykluft, T. Schwarz, M. Austinat, B. Nieswandt, H. Wiendl, and G. Stoll. 2010. Early detrimental T-cell effects in experimental cerebral ischemia are neither related to adaptive immunity nor thrombus formation. *Blood*. 115:3835–3842. http://dx.doi.org/10.1182/blood-2009-10-249078

Kleinschnitz, C., P. Kraft, A. Dreykluft, I. Hagedorn, K. Göbel, M.K. Schuhmann, F. Langhauser, X. Helluy, T. Schwarz, S. Bittner, et al. 2013. Regulatory T cells are strong promoters of acute ischemic stroke in mice by inducing dysfunction of the cerebral microvasculature. *Blood*. 121:679–691. http://dx.doi.org/10.1182/blood-2012-04-426734

Korn, T., E. Bettelli, W. Gao, A. Awasthi, A. Jäger, T.B. Strom, M. Oukka, and V.K. Kuchroo. 2007. IL-21 initiates an alternative pathway to induce proinflammatory T(H)17 cells. *Nature*. 448:484–487. http://dx.doi.org/10.1038/nature05970

Liesz, A., E. Suri-Payer, C. Veltkamp, H. Doerr, C. Sommer, S. Rivest, T. Giese, and R. Veltkamp. 2009. Regulatory T cells are key cerebroprotective immunomodulators in acute experimental stroke. *Nat. Med*. 15:192–199. http://dx.doi.org/10.1038/nm.1927

Longa, E.Z., P.R. Weinstein, S. Carlson, and R. Cummins. 1989. Reversible middle cerebral artery occlusion without craniectomy in rats. *Stroke*. 20:84–91. http://dx.doi.org/10.1161/01.STR.20.1.84

Magnus, T., H. Wiendl, and C. Kleinschnitz. 2012. Immune mechanisms of stroke. *Curr. Opin. Neurol*. 25:334–340. http://dx.doi.org/10.1097/WCO.0b013e328352ede6

Majid, A., Y.Y. He, J.M. Gidday, S.S. Kaplan, E.R. Gonzales, T.S. Park, J.D. Fenstermacher, L. Wei, D.W. Choi, and C.Y. Hsu. 2000. Differences in vulnerability to permanent focal cerebral ischemia among 3 common mouse strains. *Stroke*. 31:2707–2714. http://dx.doi.org/10.1161/01.STR.31.11.2707

McGuire, H.M., S. Walters, A. Vogelzang, C.M. Lee, K.E. Webster, J. Sprent, D. Christ, S. Grey, and C. King. 2011. Interleukin-21 is critically required in autoimmune and allogeneic responses to islet tissue in murine models. *Diabetes*. 60:867–875. http://dx.doi.org/10.2337/db10-1157

Nieswandt, B., C. Kleinschnitz, and G. Stoll. 2011. Ischaemic stroke: a thrombo-inflammatory disease? *J. Physiol*. 589:4115–4123.

Peluso, I., M.C. Fantini, D. Fina, R. Caruso, M. Boirivant, T.T. MacDonald, F. Pallone, and G. Monteleone. 2007. IL-21 counteracts the regulatory T cell-mediated suppression of human CD4+ T lymphocytes. *J. Immunol*. 178:732–739.

Shichita, T., Y. Sugiyama, H. Ooboshi, H. Sugimori, R. Nakagawa, I. Takada, T. Iwaki, Y. Okada, M. Iida, D.J. Cua, et al. 2009. Pivotal role of cerebral interleukin-17-producing gammadeltaT cells in the delayed phase of ischemic brain injury. *Nat. Med*. 15:946–950. http://dx.doi.org/10.1038/nm.1999

Spolski, R., L. Wang, C.K. Wan, C.A. Bonville, J.B. Domachowske, H.P. Kim, Z. Yu, and W.J. Leonard. 2012. IL-21 promotes the pathologic immune response to pneumovirus infection. *J. Immunol*. 188:1924–1932. http://dx.doi.org/10.4049/jimmunol.1100767

Stubbe, T., F. Ebner, D. Richter, O. Engel, J. Klehmet, G. Royl, A. Meisel, R. Nitsch, C. Meisel, and C. Brandt. 2013. Regulatory T cells accumulate and proliferate in the ischemic hemisphere for up to 30 days after MCAO. *J. Cereb. Blood Flow Metab.* 33:37–47. http://dx.doi.org/10.1038/jcbfm.2012.128

Swanson, R.A., M.T. Morton, G. Tsao-Wu, R.A. Savalos, C. Davidson, and F.R. Sharp. 1990. A semiautomated method for measuring brain infarct volume. *J. Cereb. Blood Flow Metab.* 10:290–293. http://dx.doi.org/10.1038/jcbfm.1990.47

Tzartos, J.S., M.J. Craner, M.A. Friese, K.B. Jakobsen, J. Newcombe, M.M. Esiri, and L. Fugger. 2011. IL-21 and IL-21 receptor expression in lymphocytes and neurons in multiple sclerosis brain. *Am. J. Pathol*. 178:794–802. http://dx.doi.org/10.1016/j.ajpath.2010.10.043

van Leeuwen, M.A., D.J. Lindenbergh-Kortleve, H.C. Raatgeep, L.F. de Ruiter, R.R. de Krijger, M. Groeneweg, J.C. Escher, and J.N. Samsom. 2013. Increased production of interleukin-21, but not interleukin-17A, in the small intestine characterizes pediatric celiac disease. *Mucosal Immunol*. 6:1202–1213. http://dx.doi.org/10.1038/mi.2013.19

Xie, X.J., Y.F. Ye, L. Zhou, H.Y. Xie, G.P. Jiang, X.W. Feng, Y. He, Q.F. Xie, and S.S. Zheng. 2010. Th17 promotes acute rejection following liver transplantation in rats. *J. Zhejiang Univ. Sci. B*. 11:819–827. http://dx.doi.org/10.1631/jzus.B1000030

Yilmaz, G., and D.N. Granger. 2010. Leukocyte recruitment and ischemic brain injury. *Neuromolecular Med*. 12:193–204. http://dx.doi.org/10.1007/s12017-009-8074-1

Yilmaz, G., T.V. Arumugam, K.Y. Stokes, and D.N. Granger. 2006. Role of T lymphocytes and interferon-gamma in ischemic stroke. *Circulation*. 113:2105–2112. http://dx.doi.org/10.1161/CIRCULATIONAHA.105.593046